Weierstraß–Institut
für Angewandte Analysis und Stochastik

im Forschungsverbund Berlin e.V.

A numerical simulation of the Jominy end–quench test

Dietmar Hömberg

submitted: 29th March 1995

Weierstraß–Institut
für Angewandte Analysis
und Stochastik
Mohrenstraße 39
D – 10117 Berlin
Germany

Preprint No. 144
Berlin 1995

Edited by
Weierstraß–Institut für Angewandte Analysis und Stochastik (WIAS)
Mohrenstraße 39
D — 10117 Berlin
Germany

Fax: + 49 30 2004975
e–mail (X.400): c=de;a=d400;p=iaas-berlin;s=preprint
e–mail (Internet): preprint@iaas-berlin.d400.de

A numerical simulation of the Jominy end–quench test

by D. Hömberg

Abstract

We present a numerical algorithm for simulating the Jominy end–quench test and deriving continuous cooling diagrams. The underlying mathematical model for the austenite–pearlite phase transition is based on Scheil's Additivity Rule and the Johnson–Mehl equation. For the formation of martensite we compare the Koistinen–Marburger formula with a rate law, which takes into account the irreversibility of this process.

We carry out numerical simulations for the plain carbon steels C 1080 and C 100 W 1. The results suggest that the austenite–pearlite phase change may be described decently by the Additivity Rule, except for the incubation time.

On the other hand, using a rate law to describe the martensite formation is preferable to the Koistinen–Marburger formula, which leads to unphysical oscillations of the cooling curves in simulated CCT–diagrams.

1 Introduction

In this paper we describe a mathematical model for the phase transitions in eutectoid carbon steel and use it to develop a numerical scheme for the simulation of the Jominy end–quench test.

In this test a cylindrical steel bar is heated up to its austenitic state. Then it is put in a fixation and quenched by spraying water on its lower end (cf. Fig. 1). Afterwards the hardness is measured at increasing distances from the quenched end. The results are plotted in a hardenability curve. It serves as a measure for the hardness penetration depth of this steel and thereby defines its range of application.

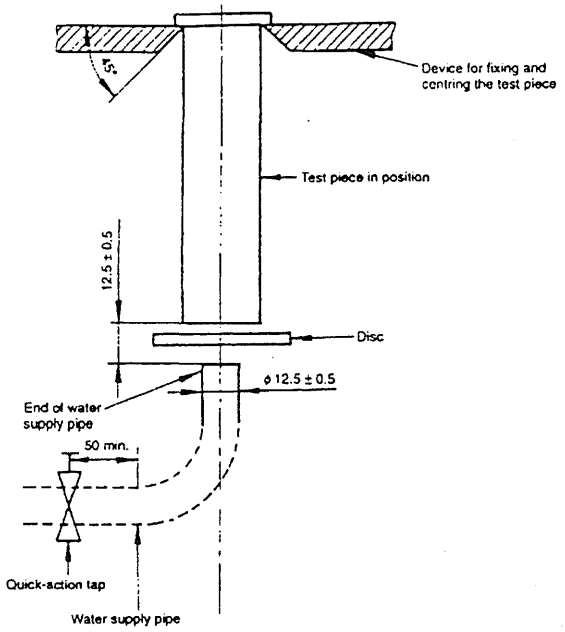

Figure 1: Diagram of the cooling device (from [19])

For a simulation of the Jominy test one first needs a mathematical model to describe the growth of pearlite and martensite as well as recalescence effects in the steel bar owing to the latent heat of the phase changes.

A lot of work has been spent on simulating phase transitions in steel, e.g. [1], [7], [12], [13], [18]. The first mathematical investigation of phase transitions in steel has been carried through by Visintin [29], but he only considered the austenite–pearlite transformation. Based on this model Verdi and Visintin [28] suggested a numerical scheme for simulating the austenite–pearlite phase change, without presenting numerical results. In [14], the author developped a model for the austenite–pearlite and the austenite–martensite phase change that is based on Scheil's Additivity Rule and the Koistinen–Marburger formula. It turned out that the Koistinen and Marburger formula is an insufficient tool for simulating the growth of martensite, since it does not take care of the irreversibility of this transition. This lead to unreasonable oscillations in the simulated CCT–diagrams.

Then in [15] the present author investigated a new model for this phase transition, where the Koistinen–Marburger formula was replaced by a rate law, accounting for the irreversibility of the martensite formation.

Here we present a numerical realization of this model and use it to simulate hardenability curves for two different plain carbon steels. In Section 2 we briefly review the mathematical model as described in [15]. In Section 3 we discuss the numerical implementation of the model. Finally, in Section 4 we discuss the results of the numerical calculations.

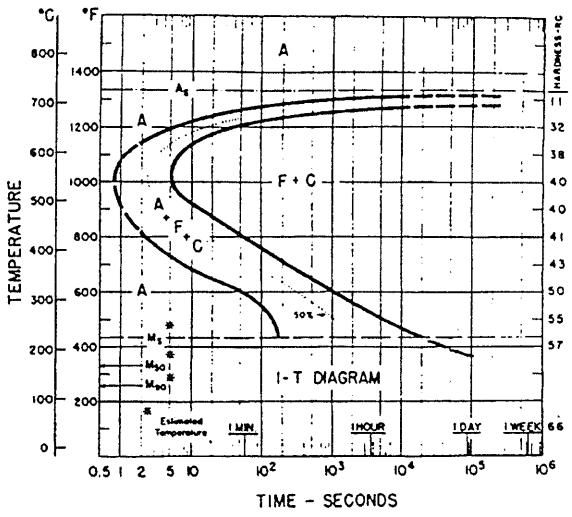

Figure 2: Isothermal–transformation diagram for the plain carbon steel C 1080 (from [2])

2 The mathematical model

2.1 Time–Temperature–Transformation diagrams

In eutectoid carbon steel two phase transitions may occur: one from austenite to pearlite and one from austenite to martensite. The A–P transformation is driven by the diffusion of carbon atoms, it is time–dependent and irreversible. The A–M transformation is diffusionless. It is temperature–dependent in such a way that the fraction of martensite only increases during non-isothermal stages of the cooling process.

The evolution of the phase transitions is usually described in Time–Temperature–Transformation diagrams. Figure 2 depicts an isothermal–transformation (IT–) diagram for the plain carbon steel C 1080. Here A_s and M_s denote the starting temperatures for the formation of pearlite and of martensite, respectively.

For fixed temperatures the bold–faced curved lines indicate the beginning of the austenite–pearlite transformation, i.e. the time when 1 per cent of the austenite has been transformed, and the end of the transformation, i.e. the time when 99 per cent of the austenite has been transformed.

In the non-isothermal case the phase evolutions are represented in a continuous–cooling–transformation (CCT–) diagram. This can be derived from an isothermal–transformation diagram by superimposing several cooling curves on it. On each curve the beginning and the end of the transformation are marked. Then the connection of the respective points defines the CCT–diagram. Compared to an IT–diagram the transformation curves are moved to later time and lower temperature (cf. Fig. 3).

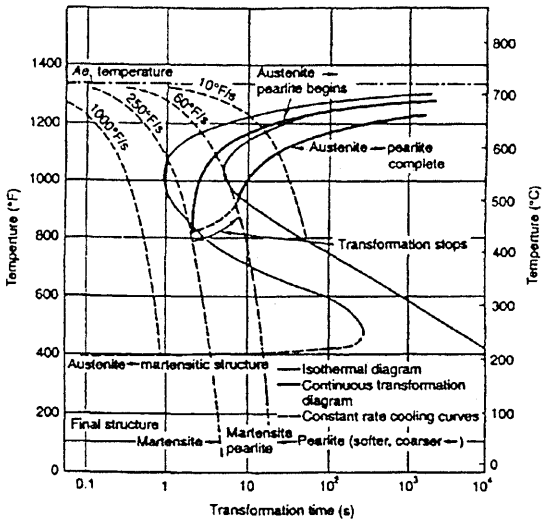

Figure 3: Derivation of a continuous–cooling from an isothermal–transformation diagram (from [4])

2.2 The austenite–pearlite phase change

As the A–P transformation is a nucleation and growth process, it is governed by the nucleation rate (the amount of nuclei of the new phase formed per unit time and volume) and by the growth rate of the nuclei.
Assuming these rates to be constant and furthermore spherical growth of the nuclei, Johnson and Mehl [21] in 1939 derived the equation

$$p(t) = 1 - e^{-\frac{\pi}{3}\dot{N}G^3t^4} \tag{2.1}$$

for the A–P transformation in the isothermal case. Here p is the fraction of pearlite, $\dot{N}$ is the nucleation rate and G is the growth rate of the nuclei.
As in [1] and [29] we use (2.1) in the parametric version

$$p(t) = 1 - e^{-b(T)t^{a(T)}}. \tag{2.2}$$

The temperature dependent coefficients $a(T)$ and $b(T)$ can easily be calculated using the transformation curves in the IT–diagram (cf. Section 2.3).
In the non-isothermal case, we use the *additivity rule* to describe the formation of pearlite:

$$\int_0^t \frac{1}{\tau(T(\xi), p(t))}\, d\xi = 1. \tag{2.3}$$

Here $\tau(T, p)$ denotes the time to transform the fraction p to pearlite at constant temperature T. Thus, by (2.2),

$$\tau(T, p) = \left(-\frac{\ln(1-p)}{b(T)}\right)^{\frac{1}{a(T)}}. \tag{2.4}$$

Equation (2.4) was derived by Scheil [26] to predict the incubation period of the A–P transformation. Later Avrami [5] and Cahn [8] showed that (3.4) can be applied to characterize the kinetics of a class of phase changes which they called *additive*.
Although the pearlite phase change is not an additive transformation in their sense, (cf. [9]), according to a comparative investigation by Hayes [11] the additivity rule is a better tool for predicting the course of the phase change than a rate law. Moreover, measurements by Hawbolt et al. [12] show that also in quantity the A–P transformation is described well by the additivity rule, except for the incubation period where the pearlite fraction predicted by the additivity rule shows only poor coincidence with the measurements. It should be noticed that equations of this type are also used for modelling fatigue effects, e.g. the *Palmgren–Minor rule* (cf. [6]).
A different approach to model a nucleation and growth process was chosen by Andreucci et al. [3]. Going back to the ideas of Johnson and Mehl they derived an integral equation to describe the solidification of polymers in the non-isothermal case.

2.3 Identifying coefficients from IT–diagrams

Assuming that the generalized Johnson –Mehl–equation (2.2) appropriately describes the isothermal evolution of the phase fractions we present a simple method to obtain the data functions $a(T)$ and $b(T)$ from the IT–diagrams.
Since the bold–faced curves in these diagrams are the 'iso–fractions' $p = 0.01$ and $p = 0.99$, we interpret these transformation curves as the respective graphs of functions

$$t_s : [M_s, A_s] \to \mathbb{R}_+, \quad t_f : [M_s, A_s] \to \mathbb{R}_+,$$

which measure the beginning and end of the pearlitic transformation for given temperature. These data functions can be drawn from the IT–diagram. Then the wanted coefficients are the solution to the following nonlinear system of equations:

$$0.01 = 1 - e^{-b(T)t_s^{a(T)}} \tag{2.5a}$$

$$0.99 = 1 - e^{-b(T)t_f^{a(T)}} \tag{2.5b}$$

Simple manipulations show that the solution is given by

$$a(T) = \frac{\ln(\ln(0.01)) - \ln(\ln(0.99))}{\ln(t_f(T)) - \ln(t_s(T))} \tag{2.6a}$$

$$b(T) = -\ln(0.99)t_f(T)^{-a(T)}. \tag{2.6b}$$

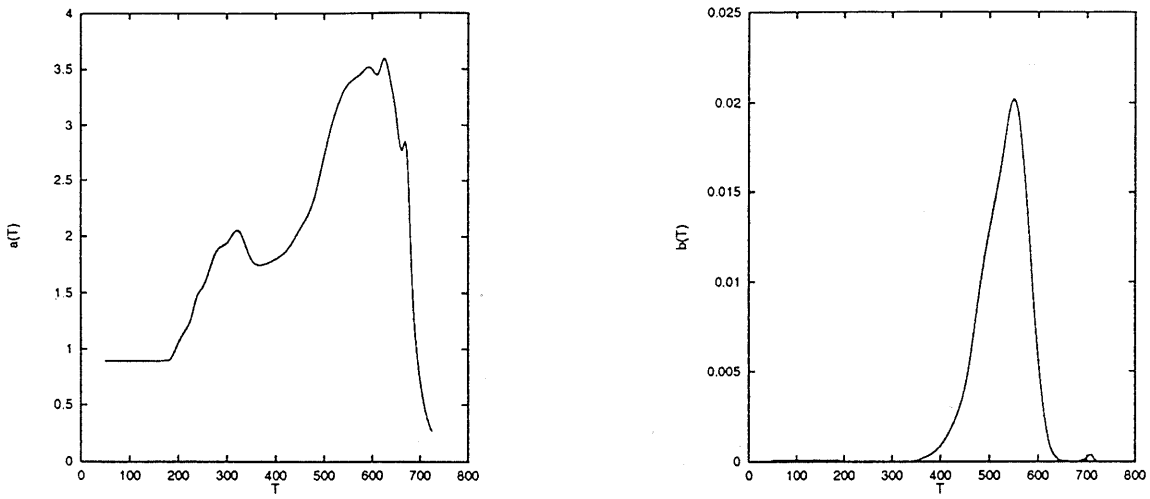

Figure 4: The data functions $a(T)$ and $b(T)$ for the carbon steel C 1080.

Figure 4 shows the behaviour of the coefficients $a(T)$ and $b(T)$ in the temperature range $[M_f, A_s]$ for the plain carbon steel C 1080. For temperatures below M_s the values are obtained by linear extrapolation. Although it cannot be concluded from the diagram, also b stays positive in the whole temperature range. Hence in the following we assume a and b to be continuous functions on $[M_f, A_s]$, bounded away from zero.

2.4 An Initial Value Problem for the A–P transformation

A simple way to exploit the additivity rule is to differentiate it formally with respect to time. Since we get an inner derivative $\dot{p}$, rearranging terms leads to the following initial value problem:

$$p(0) = p_0 \tag{2.7a}$$
$$\dot{p}(t) = \hat{f}(t, p(t), T), \tag{2.7b}$$

with

$$\hat{f}(t, p(t), T) = -\Big(\int_0^t \frac{\partial}{\partial p} \frac{d\xi}{\tau(T(\xi), p(t))} \Big)^{-1} \frac{1}{\tau(T(t), p(t))}. \tag{2.8}$$

It may be proved (cf. [14]) that for any given (integrable) temperature evolution $T : [0, t_E] \to [M_f, A_s]$, (2.7a,b) admits a unique solution p, satisfying

$$0 \le p(t) \le c_{t_E} < 1, \quad \text{for all } t \in [0, t_E], \tag{2.9}$$

with a constant c_{t_E}, depending only on the end time t_E. Moreover, we have

$$\dot{p}(t) \ge 0, \tag{2.10}$$

i.e. the irreversibility of the austenite–pearlite transformation carries over to the model.

Unfortunately, as figure 4 shows, the coefficient a, which was equal to 4 in the original Johnson–Mehl equation and assumed to be greater than 1 in [28] and [29], actually takes values less then 1, if the temperature is in a range just below A_s. In this case, we can prove the following

Proposition 2.1 *Let $T : [0, t_E] \to [M_f, A_s]$ be a continuous function, such that*

$$a(T(t)) < 1 \quad \text{for all } 0 \leq t \leq \tilde{t},$$

then the following are valid:

$$\lim_{t \to 0(+)} p(t) = 0, \tag{2.11a}$$

$$\lim_{t \to 0(+)} \dot{p}(t) = \infty. \tag{2.11b}$$

For the proof, we refer to [14].
In a nucleation and growth process the increase of the volume fraction of the new phase should be 'small' during the incubation time, which is a contradiction to (2.11b). Thus, Proposition 2.1 gives the mathematical reason, why the additivity rule does not work well for the early stages of the transformation. As said before, this fact has also been observed experimentally.
To overcome this difficulty, we adopt the following philosophy: We define an incubation time t_I, which we keep fixed. Giving up the aim of predicting the exact evolution kinetics during this incubation time, we just gauge the process by demanding that the additivity rule shall hold, when the end of the incubation time is reached. This leads to the following model:

- Let $T : [0, t_E] \to \mathbb{R}$ be a given temperature evolution,
- $t_I \in (0, t_E)$ the fixed incubation time, then, depending on T,
- p_0 is defined by

$$\int_0^{t_I} \frac{1}{\tau(T(\xi), p_0)} \, d\xi = 1. \tag{2.12}$$

- The fraction of pearlite is determined by the following initial value problem (IVP):

$$p(0) = p_0, \tag{2.13a}$$

$$\dot{p}(t) = \begin{cases} 0 & , 0 < t \leq t_I \\ \hat{f}(t, p(t), T) H(A_s - T(t)) & , t_I < t < t_E. \end{cases} \tag{2.13b}$$

The heaviside function

$$H(x) = \begin{cases} 1, & x > 0 \\ 0, & x \leq 0 \end{cases}$$

prevents the formation of pearlite above the critical temperature A_s.

2.5 The austenite–martensite phase change

While the additivity rule is a well investigated decent tool for describing the growth of pearlite, there seems to be no satisfactory model at hand for the martensitic transformation in steel.
Usually, exponential growth laws like the Koistinen and Marburger formula

$$m(t) = 1 - e^{-c(M_s - T(t))} \tag{2.14}$$

are used (cf. [14], [16], [17]).
These equations have all in common that they do not model the irreversibility of the austenite – martensite phase transition. Thus, in numerical simulations based on these models, owing to the release of latent heat, usually a decrease in the martensite fraction is observed (cf. [14] and Section 4).
The formation of martensite starts below the critical temperature M_s, and the volume fraction of martensite only grows during non-isothermal stages of a cooling process.
Hence we propose the following rate law for the growth of martensite:

$$m(0) = 0, \tag{2.15a}$$
$$\dot{m}(t) = (1 - m(t))G(T(t))H(-T_t(t)). \tag{2.15b}$$

Here, again H is the heaviside function. G shall be bounded, positive and (Lipschitz–) continuous, satisfying $G(x) = 0$ for all $x \geq M_s$.
If during some stage of a heat treatment cycle either $T \geq M_s$ or T is increasing, i.e. $T_t \geq 0$, according to (2.15b) we have $\dot{m}(t) = 0$, whence no martensite is produced during this stage.
Moreover, since $\dot{m} \geq 0$, the irreversibility of the martensite transformation is now incorporated in the model.
Putting $m(0) = 0$, we tacitly assume that we start with a temperature $T(0) > M_s$.

2.6 The complete model

In (2.13b) and (2.15b), actually, not the fractions p and m occur but the volume fraction of austenite which is $1 - p$ or $1 - m$, respectively. Therefore, to combine both models one only has to replace these terms by the volume fraction of austenite in the case when both pearlite and martensite are present, i.e. $1 - p - m$.
So we end up with the following initial value problem for the phase transitions in eutectoid carbon steel:

$$
\begin{aligned}
p(0) &= p_0, && (2.16a)\\
m(0) &= 0, && (2.16b)\\
\dot{p}(t) &= (1-p(t)-m(t))\, f(t,p(t),m(t),T)\, H(A_s - T(t)), && (2.16c)\\
\dot{m}(t) &= (1-p(t)-m(t))\, G(T(t))H(-T_t(t)), && (2.16d)
\end{aligned}
$$

where we define

$$
f(t,p,m,T)) := -\Big(\int_0^t \frac{d\xi}{a(T(\xi))\tau(T(\xi),p,m)}\Big)^{-1} \frac{\ln(1-p-m)}{\tau(T(t),p,m)})H(t-t_I). \tag{2.17}
$$

Here, $\tau(T,p,m)$ is defined by

$$
\tau(T,p,m) = \Big(-\frac{\ln(1-p-m)}{b(T)}\Big)^{\frac{1}{a(T)}}. \tag{2.18}
$$

The following Proposition summarizes the properties of the preceding model.

Proposition 2.2 *Let $T : [0,t_E] \to \mathbb{R}$ be an integrable and (weakly) differentiable temperature evolution with $\theta(0) = A_s$, and $t_I \in (0,T)$ the fixed incubation time. Then the following are valid:*

(1) p_0 is uniquely defined by

$$
\int_0^{t_I} \frac{1}{\tau(T(\xi),p_0)}\, d\xi = 1.
$$

(2) The IVP (2.16a–d) has a unique (absolutely) continuous solution (p,m).

(3) $$p_0 \le p(t) + m(t) \le c_{t_I,t_E} < 1 \text{ for all } t \in [0,t_E].$$

See [15] for the proof and the precise formulation of the necessary assumptions.

2.7 Three-dimensional case

Let $\Omega \subset \mathbb{R}^3$ be bounded with smooth boundary $\partial\Omega =: \Gamma$ and $Q := \Omega \times (0,t_E)$.
As mechanical effects are neglected in this paper, using Fourier's law of heat conduction, we get the following balance of energy:

$$
\rho\frac{\partial e}{\partial t} - \nabla\cdot(k\nabla T) = 0, \tag{2.19}
$$

where ρ is the mass density, e the specific internal energy and k the heat conductivity of the material under consideration.

In a spatial model the propagation of latent heat released during the phase changes has to be considered. Following [30], it is assumed that there exists a differentiable material function $\hat{e}$ such that the internal energy takes the form

$$e(x,t) = \hat{e}(T,p,m), \tag{2.20}$$

with the partial derivatives

$$\frac{\partial \hat{e}}{\partial T} = c, \quad \frac{\partial \hat{e}}{\partial p} = -L_p, \quad \frac{\partial \hat{e}}{\partial m} = -L_m. \tag{2.21}$$

Here c denotes the specific heat at constant pressure and L_p, L_m denote the latent heats of the austenite–pearlite and the austenite–martensite phase change, respectively.
ρ, c, L_p, L_m shall not depend on the phase fractions p, m. Thus we obtain the following balance of energy:

$$\rho(T)c(T)\frac{\partial T}{\partial t} - \nabla \cdot (k(T)\nabla T) = \rho(T)L_p(T)\frac{\partial p}{\partial t} + \rho(T)L_m(T)\frac{\partial m}{\partial t}, \qquad \text{in } Q, \tag{2.22}$$

together with boundary and initial conditions

$$-k(T)\frac{\partial T}{\partial \nu} = \gamma(T)(T - T_\Gamma), \qquad \text{in } \Gamma \times (0,t_E), \tag{2.23a}$$

$$T(.,0) = A_s, \qquad \text{in } \Omega. \tag{2.23b}$$

Here, T_Γ is the outside temperature and γ the heat exchange coefficient.
For further mathematical analysis, we assume that ρ, c, k, γ are positive constants and that the latent heats L_p, L_m are positive, bounded (Lipschitz–) continuous functions. The assumptions on ρ, c and k can be weakened, but, of course, help to simplify the analysis.
In addition, we replace the heaviside function with the following regularized version (cf. fig. 5):

$$H_\delta(x) = \begin{cases} 0, & x < 0, \\ \frac{1}{\delta}x, & 0 \le x < \delta, \\ 1, & x \ge \delta, \end{cases} \tag{2.24}$$

where $\delta > 0$ is a 'small' parameter. Introducing the further notation $A_\delta(.) := -H_\delta(-.)$, and using (2.16a–d) we end up with the following nonlinear parabolic problem (P_δ) for phase transitions in eutectoid carbon steel:

$$\rho c T_t + \rho L_m(T)(1-p-m)G(T)A_\delta(T_t) - k\Delta T = \rho L_p(T)p_t, \qquad \text{in } Q, \tag{2.25a}$$

$$-k\frac{\partial T}{\partial \nu} = \gamma(T - T_\Gamma), \qquad \text{in } \Gamma \times (0,t_E), \tag{2.25b}$$

$$T(.,0) = A_s, \qquad \text{in } \Omega. \tag{2.25c}$$

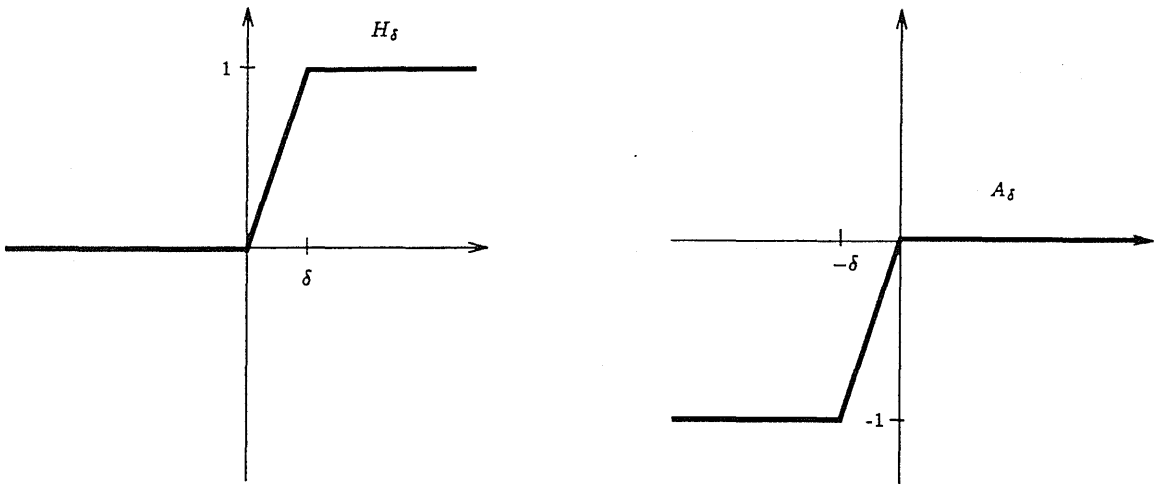

Figure 5: The functions H_δ and A_δ.

Here, for almost all $x \in \Omega$, $\big(p(x,.), m(x,.)\big)$ is the solution to the following (IVP):

$$p(x,0) = p_0(T(x,.)), \qquad (\text{ cf. (2.12) }) \tag{2.25d}$$

$$m(x,0) = 0, \tag{2.25e}$$

$$p_t(x,t) = \big(1 - p(x,t) - m(x,t)\big) f(t, p(x,t), m(x,t)T(x,.)) H_\delta(A_s - T(x,t)), \tag{2.25f}$$

$$m_t(x,t) = \big(1 - p(x,t) - m(x,t)\big) G(T(x,t)) H(-T_t(x,t)). \tag{2.25g}$$

The following theorem shows that problem (P_δ) is well-posed:

Theorem 2.1 *Assume that the incubation time t_I has been chosen small enough, then (P_δ) has a unique solution (T,p,m), where the phase fractions (p,m) satisfy the properties of proposition 2.2.*

For a precise formulation of the assumptions on the data and for the proof we again refer to [15].
Instead of assuming the incubation time t_I to be chosen 'small enough' one could also demand $\frac{\partial m}{\partial t} = 0$ a.e. in $(0,t_I)$ or $p_0 \in (0,1)$ constant, independent of T.
The first case refers to a heat treatment with a moderate cooling rate, producing pearlite and subsequently possibly some martensite.
The second condition applies to quench cooling, i.e. very fast cooling to achieve a nearly pure martensitic structure. In this case it is reasonable to assume p_0 to be constant, because no more pearlite will be formed during the cooling process.
From a mathematical point of view it is interesting to see what happens if the regularization parameter δ tends to zero. This question has been investigated in [15], we only want to remark here that one still gets a solution in this case.

3 Numerical method

3.1 The algorithm

In this section we will apply our model to simulate the Jominy end–quench test. Owing to the symmetries of the problem (cf. Fig. 1), we make use of cylindrical coordinates. Thus, we obtain the following energy balance:

$$A(T)T_t - k\Big(T_{rr} + \frac{1}{r}T_r + T_{zz}\Big) = B(T), \quad \text{in } \Omega \times (0,T), \tag{3.1}$$

with $\Omega = (0,R) \times (0,H)$, where R is the radius and H the height of the steel bar. Moreover we have used the abbreviations

$$A(T) = \rho(T)c(T) \tag{3.2}$$

$$B(T) = \rho(T)L_p(T)f_1(p,m,T) + \rho(T)L_m(T)f_2(p,m,T), \tag{3.3}$$

where f_1 anf f_2 are the right–hand sides in (2.25f,g).
According to Figure 6, we consider the following boundary conditions:

$$-k\frac{\partial T}{\partial \nu} = \begin{cases} \kappa(T - T_W), & \text{in } \Gamma_1 \times (0,t_E), \\ \sigma(T^4 - T_L^4), & \text{in } \Gamma_2 \times (0,t_E), \\ 0, & \text{in } \Gamma_3 \times (0,t_E), \\ 0, & \text{in } \Gamma_4 \times (0,t_E). \end{cases} \tag{3.4}$$

Here, T_W and T_L denote the temperatures of water and the surrounding air, respectively. We will approximate the solution to (3.1), (3.4) by using a semi-implicit Crank–Nicholson scheme. Defining

$$t_j = j \cdot \delta t, \quad j = 0, \ldots, N_t, \tag{3.5}$$

$$r_\mu = \mu \cdot \delta r, \quad \mu = 0, \ldots, N_r, \tag{3.6}$$

$$z_\nu = \nu \cdot \delta z, \quad \nu = 0, \ldots, N_z, \tag{3.7}$$

we obtain a lattice on $\Omega \times (0,t_E)$ with the mesh sizes

$$\delta t = \frac{t_E}{N_t}, \quad \delta r = \frac{R}{N_r}, \quad \delta z = \frac{H}{N_z}. \tag{3.8}$$

Let $T_{\mu,\nu,j}$ be an approximation of $T(r_\mu, z_\nu, t_j)$, then, for $0 < j < N_t, 0 < \mu < N_r, 0 < \nu < N_z$ we consider the following Crank-Nicholson scheme:

$$A(T_{\mu,\nu,j})\frac{T_{\mu,\nu,j+1} - T_{\mu,\nu,j}}{\delta t} = \frac{k}{2}\theta^{j+1} + \frac{k}{2}\theta^j + B(T_{\mu,\nu,j}), \tag{3.9}$$

with

$$\theta^j = \frac{T_{\mu+1,\nu,j} - 2T_{\mu,\nu,j} + T_{\mu-1,\nu,j}}{(\delta r)^2} + \frac{1}{\mu\delta r}\frac{T_{\mu+1,\nu,j} - T_{\mu-1,\nu,j}}{2\delta r} + \frac{T_{\mu,\nu+1,j} - 2T_{\mu,\nu,j} + T_{\mu,\nu-1,j}}{(\delta z)^2}. \tag{3.10}$$

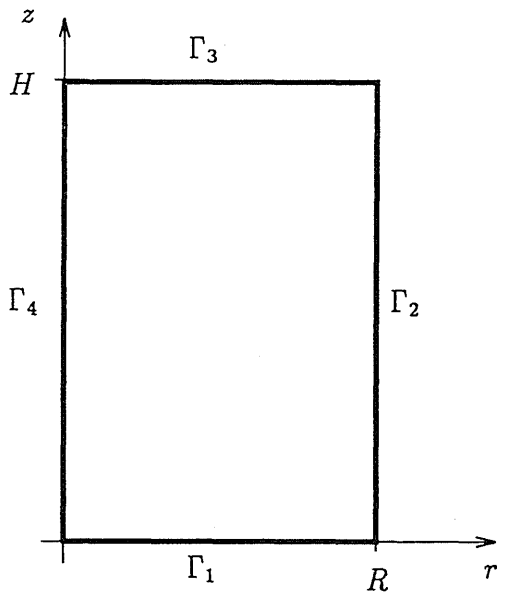

Figure 6: Half the cross section of a cylindrical steel bar with height H and radius R.

Linearizing the radiation condition on Γ_2, we incorporate the boundary conditions in the usual way. Owing to the linearization

$$T(r,z,t) = T(0,z,t) + rT_r(0,z,t) \tag{3.11}$$

for $r << 1$ and arbitrary z and t, using the boundary condition on Γ_4, we get

$$\frac{1}{r}\frac{\partial T}{\partial r} \approx 0, \text{ for } r << 1. \tag{3.12}$$

Next, we introduce the transformation

$$i = \mu(N_r+1) + \nu + 1, \quad 0 \le \mu \le N_r, \quad 0 \le \nu \le N_z \tag{3.13}$$

and the vector $T^j \in \mathbb{R}^N, N = (N_r+1)(N_z+1)$, defined by

$$T_i^j = T_{\mu,\nu,j}i \qquad 1 \le i \le N. \tag{3.14}$$

Then, in order to find a solution to the semi implicit scheme (3.9), in each time step j we have to solve the linear system

$$A^j T^{j+1} = B^j. \tag{3.15}$$

Defining j_I by

$$j_I \cdot \delta t = t_I, \tag{3.16}$$

and assuming that no martensite will be formed during the first j_I steps we end up with the following algorithm:

Initialize

$$\begin{aligned} T^0 &= A_s \\ A_i^0 &= \rho(T_i^0)c(T_i^0) \\ p^0 &= 0 \\ m^0 &= 0 \\ B^0 &= 0 \end{aligned}$$

For $j = 0$ to $j_I - 2$ do

solve $A^j T^{j+1} = B^j$

$$\begin{aligned} m^{j+1} &= 0 \\ p^{j+1} &= 0 \\ B^{j+1} &= 0 \\ A_i^{j+1} &= \rho(T_i^{j+1})c(T_i^{j+1}) \end{aligned}$$

For $j = j_I - 1$ do

solve $A^j T^{j+1} = B^j$

calculate initial value $p_{0,i}$ by applying Newton's method to

$$H(p) = \delta t \sum_{k=1}^{j_I-1} \frac{1}{\tau(T_i^k, p)} + \frac{\delta t}{2}\frac{1}{\tau(T_i^0, p)} + \frac{\delta t}{2}\frac{1}{\tau(T_i^{j_I}, p)} - 1$$

$p^{j+1} = p_0$

$m^{j+1} = 0$

calculate B^{j+1}, A^{j+1}

For $j = j_I$ to $N_t - 1$ do

solve $A^j T^{j+1} = B^j$

calculate m^{j+1}, p^{j+1}

calculate A^{j+1}, B^{j+1}.

The most time–consuming part of the algorithm is the numerical approximation of (2.17). In each time step a new value for p occurs in the integrand. Hence the integrand has to be evaluated completely in each time step, whereby the computing effort to approximate the integral increases quadratically in time.
To avoid a further increase in computing time, for the calculation of (p^{j+1}, m^{j+1}) an explicit single-step method was used.

3.2 Physical parameters

The data for specific heat c and density ρ have been taken from tables in [10]. The heat conductivity has been calculated according to Simidu's formula (cf. [10]):

$$k = 1.16 \cdot \left(60.0 - 8.7C - 14.4Mn - 29.0Si\right) \quad \frac{J}{m\,s\,K}, \tag{3.17}$$

where C, Mn, Si are the volume fractions of carbon, manganese and silicon for the respective steel.
For the latent heats we take the values from [13]:

$$L_p = 77.0\frac{J}{g}, \qquad L_m = 84.0\frac{J}{g}. \tag{3.18}$$

According to literature (cf. [20]), the heat transfer coefficient γ during spray water cooling lies in the range

$$1000\frac{W}{m^2\,K} \leq \gamma \leq 3000\frac{W}{m^2\,K}. \tag{3.19}$$

For our simulations we use values for γ which are larger than the upper bound in (3.19). Finally, the temperature thresholds A_s, M_s can be drawn from the respective IT–diagram.

4 Numerical simulations

4.1 Results for the steel C 1080

First, we applied our numerical scheme to the eutectoid carbon steel C 1080 from [2] (see Fig. 2). For the heat exchange coefficient γ we used the value $\gamma = 8.0 \cdot 10^3 W/m^2K$.
Figure 7 depicts the general course of the simulation. At the lower quenched end of the steel bar, martensite begins to grow while in the upper part pearlite starts to form.
Figure 8 shows the corresponding CCT-diagram. As expected, the curves are moved to later time and lower temperature. The bucklings of the cooling curves between the transformation lines indicate the release of latent heat during the formation of pearlite. In Fig. 8(a), we used the Koistinen–Marburger formula (cf. (2.14)) to describe the evolution of the martensite fraction. Instead of intersecting the dotted M_s–line only once, the cooling curves go up again. To prevent repeated oszillations we even had to cut the latent heat L_p in halves.
To overcome this unphysical behaviour, we replaced the Koistinen–Marburger formula with a rate law, which takes care of the irreversibility of the phase change (cf. (2.15a,b)). The resulting CCT-curve is depicted in Fig. 8(b). Using the original value for L_p, the cooling curves intersect the M_s–line only once without performing unreasonable heating-up effects.
Finally, Figure 9 shows the hardenability curve for C 1080 side by side with a diagram in which the martensite fraction is plotted against the distance from the quenched end. Obviously, pearlite also has a certain hardness, so one can only expect that both curves coincide for small distances from the quenched end, which is the case.

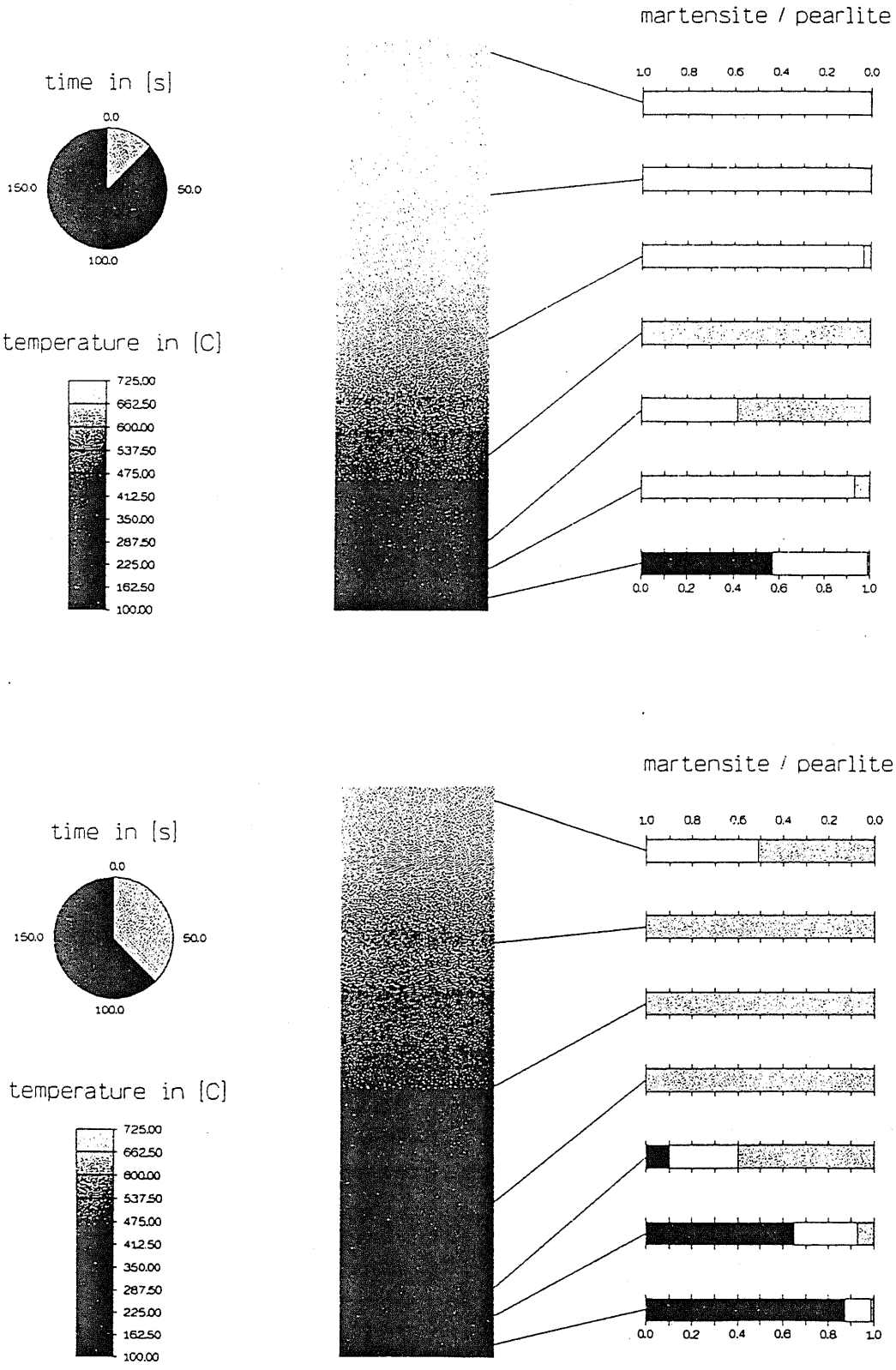

Figure 7: Numerical simulation of the Jominy test for the steel C 1080 after 25 s (top) and after 75 s (bottom).

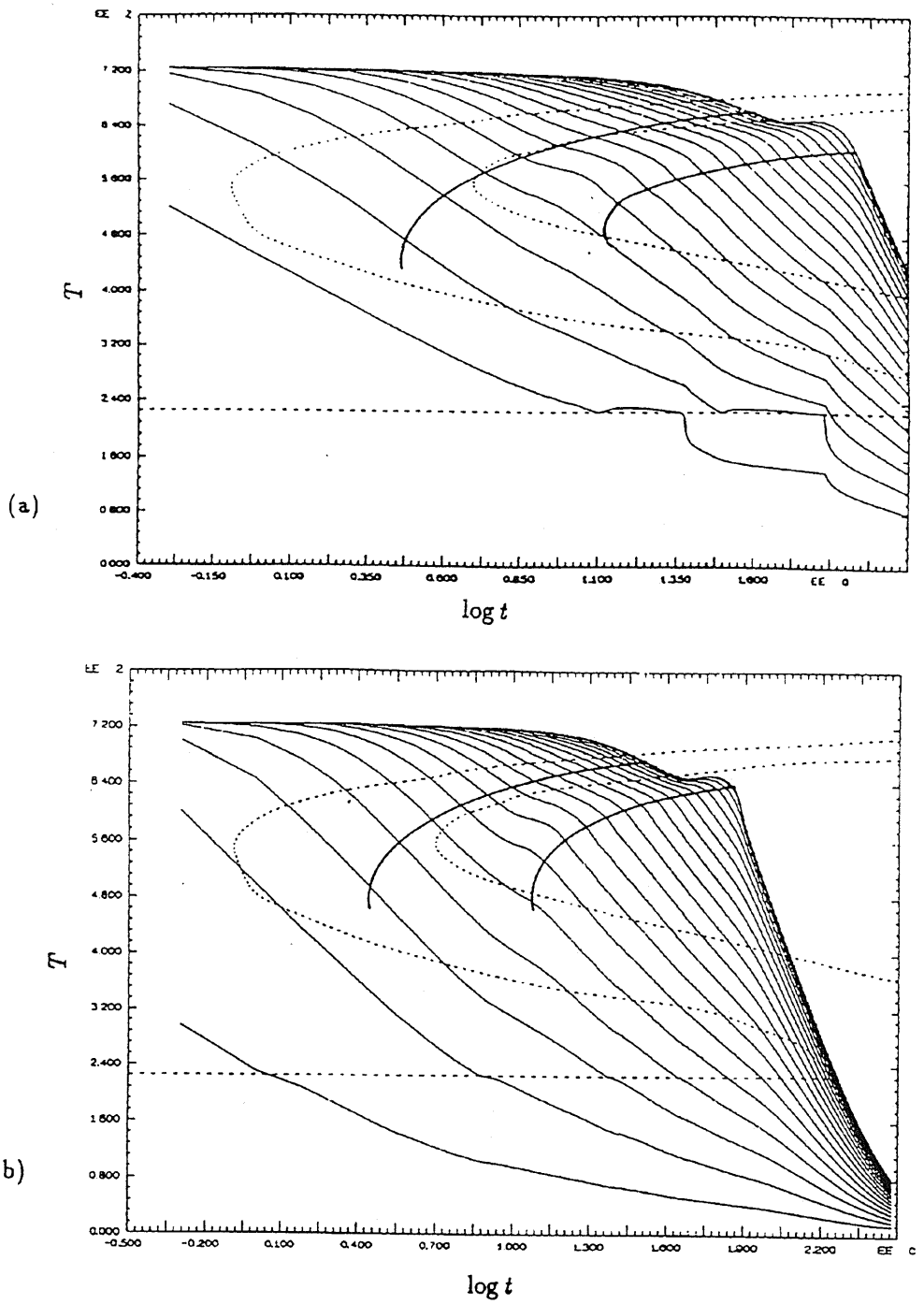

Figure 8: Numerical simulation of a CCT–diagram for the steel C 1080: (a) using the Koistinen–Marburger formula, (b) using a rate law to describe the martensite fraction.

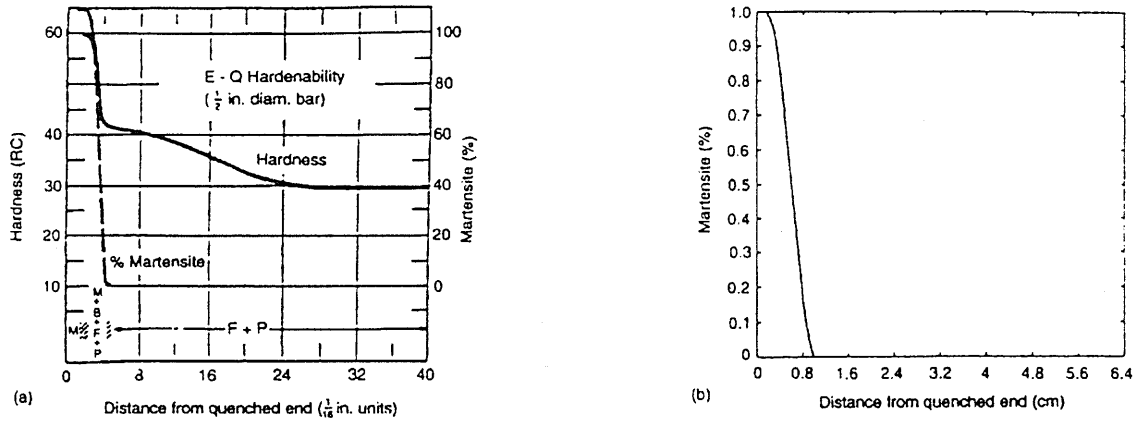

Figure 9: (a) Hardenability curve for the steel C 1080 (from [2]), (b) numerically calculated martensite fraction plotted against the distance from the quenched end.

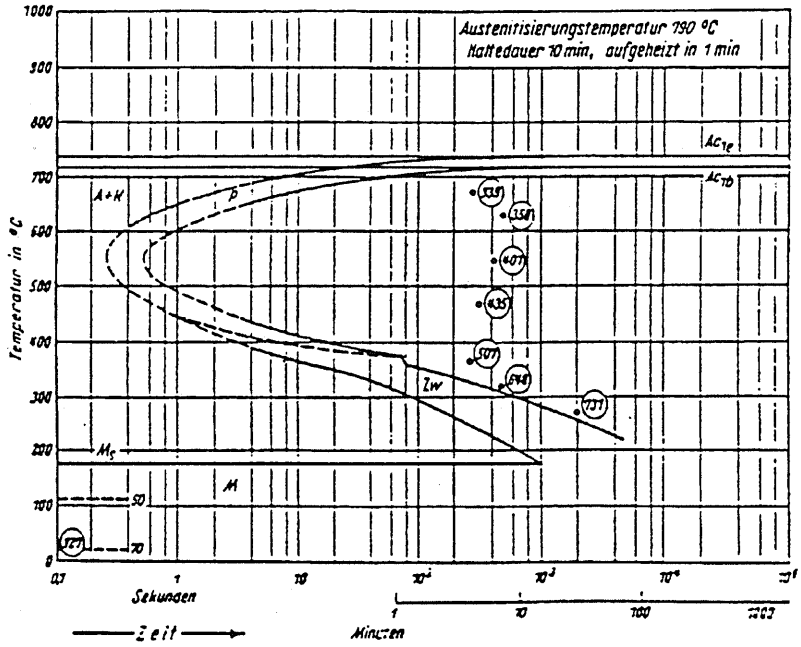

Figure 10: IT–diagram for the steel C 100 W 1 (from [25]).

4.2 Results for the steel C 100 W 1

In a second simulation, we applied our scheme to the steel C 100 W 1 from [25]. Although this steel has a carbon content of 1.0%, during continous cooling it only performs the eutectoid transformation. Thus the application of our model is justified.

Fig. 10 shows the IT–diagram for this steel. The pearlite transformation starts much earlier than in the case of the steel C 1080.

For the heat exchange coefficient we used the value $\gamma = 4.0 \cdot 10^4 W/m^2 K$.

Figure 11 depicts the numerically simulated CCT-diagram for C 100 W 1 using the rate

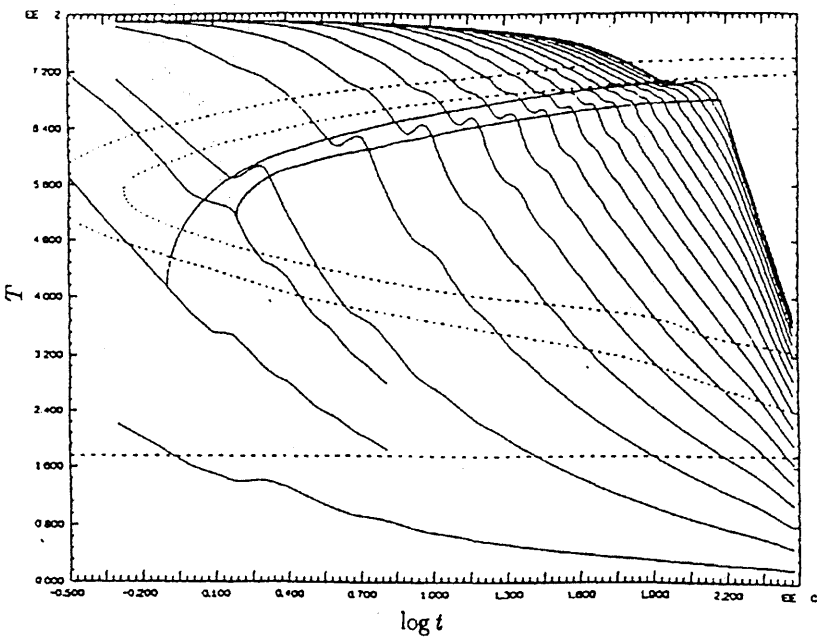

Figure 11: Numerical simulation of a CCT–diagram for the steel C 100 W 1.

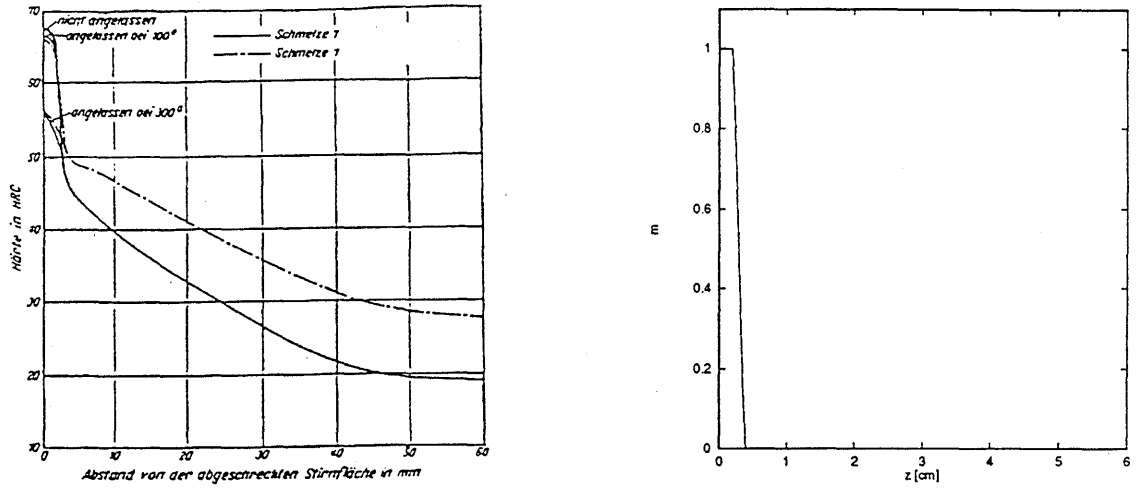

Figure 12: Hardenability curve for the steel C 100 W 1 (from [25]), left; numerically calculated martensite fraction plotted against the distance from the quenched end, right.

law (2.15a,b). Here, the influence of the latent heat of the pearlitic transformation is more destinct than in Fig. 8.

Finally, Fig. 12 shows that also for C 100 W 1 the numerically calculated martensite fraction plotted against the distance from the quenched end is in good agreement with the respective hardenability curve from [25].

5 Conclusions

The numerical results show that the algorithm is capable of reproducing the hardenability curve for a steel, provided that the heat exchange coefficient has been adequately chosen. In order to make our model utilizable for practical applications, it first has to be extended to a broader class of steels.
Therefore, the formation of ferrite and bainite has to be incorporated. This phase transitions can be modelled similarly to the growth of pearlite.
A further interesting line of research is to incorporate the reverse transformation to austenite, including hysteresis effects. Then one would be able to simulate complete heat treatment cycles, giving rise to a lot of practical applications.

References

[1] Agarwal, P. K., Brimacombe, J. K., *Mathematical Model of Heat Flow and Austenite-Pearlite Transformation in Eutectoid Carbon Steel Rods for Wire*, Metall. Trans. B, 12 (1981), 121-133.

[2] American Society for Metals, *Atlas of Isothermal Transformation and Cooling Transformation Diagrams*, Ohio, 1977.

[3] Andreucci, D., Fasano, A., Primicerio, M., *On a Mathematical Model for the Crystallization of Polymers*, in: o'Malley, R. E. (Ed..), *Proc. ICIAM 1991*, SIAM, Philadelphia, 1992, 99-118.

[4] Avner, S. H., *Introduction to physical metallurgy*, McGraw–Hill, Tokyo, 1974.

[5] Avrami, M., J. Chem. Phys., 8 (1940), 812-819.

[6] Bergmann, J., Seeger, T., *Über neuere Verfahren der Anrißlebensdauervorhersage für schwingbelastete Bauteile auf der Grundlage örtlicher Belastungen*, Z. Werkstofftech., 8 (1977), 89-100.

[7] Buza, G., Hougardy, H. P., Gergely, M., *Calculation of the isothermal transformation diagram from measurements with continuous cooling*, Steel Res., 57 (1986), 650-653.

[8] Cahn, J. W., *Tranformation Kinetics during Continuous Cooling*, Acta Met., 4 (1956), 572-575.

[9] Christian, J. W., *The Theory of Transformations in Metals and Alloys*, Pergamon Press, Oxford, 1975.

[10] Energie– und Betriebswirtschaftsstelle des Vereins Deutscher Eisenhüttenleute, *Anhaltszahlen für die Wärmewirtschaft in Eisenhüttenwerken*, Verlag Stahleisen mbH, Düsseldorf, 1968.

[11] Hayes, W.J., *Mathematical Models in Materials Science*, M. Sc. Thesis, Oxford, 1985.

[12] Hawbolt, E. B., Chau, B., Brimacombe, J. K., *Kinetics of Austenite-Pearlite Transformation in Eutectoid Carbon Steel*, Metall. Trans. A, 14 (1983), 1803-1815.

[13] Hengerer, F., Strässle, B., Bremi, P., *Berechnung der Abkühlvorgänge beim Öl– und Lufthärten zylinder- und plattenförmiger Werkstücke aus legiertem Vergütungsstahl mit Hilfe einer elektronischen Rechenanlage*, Stahl u. Eisen 89 (1969), 641–654.

[14] Hömberg, D., *A mathematical model for the phase transitions in eutectoid carbon steel*, IMA J. Appl. Math., 54 (1995), 31–57.

[15] Hömberg, D., *Irreversible phase transitions in steel*, WIAS Preprint No. 131, 1994.

[16] Hornbogen, E., Skrotzki, B., *Fractality and reversibility of ferrous martensite*, Steel Res., 63 (1992), 348–353.

[17] Hougardy, H. P., *Darstellung der Umwandlungen für technische Anwendungen und Möglichkeiten ihrer Beeinflussung* in *Werkstoffkunde Stahl. Bd. 1. Grundlagen*, Springer Verlag, Berlin, 1984, 198-231.

[18] Hougardy, H. P., Yamazaki, K., *An improved calculation of the transformation of steels*, Steel Res., 57 (1986), 466-471.

[19] International Organization for Standardization, *International Standard 642, Steel – Hardenability test by end quenching (Jominy test)*, 1979.

[20] Jeschar, R., Scholz, R., Reiners, U., Maaß, R., *Kühltechniken zur thermischen Behandlung von Werkstoffen*, Stahl u. Eisen, 107 (1987), 251–258.

[21] Johnson, W. A., Mehl, R. F., Trans. Amer. Inst. min. metallurg. Eng., Iron Steel Div., 135 (1939), 416-458.

[22] Koistinen, D. P., Marburger, R. E., *A general equation prescribing the extent of the austenite-martensite transformation in pure iron-carbon alloys and plain carbon steels*, Acta Met., 7 (1959), 59-60.

[23] Ladyženskaja, O. A., Solonnikov, V. A., Ural'ceva, N. N., *Linear and Quasilinear Equations of Parabolic Type*, Amer. Math. Soc., Providence, R.I., 1988.

[24] Lions, J. L., Magenes, E., *Non-Homogenous Boundary Value Problems and Applications, Vol. II,* Springer Verlag, Berlin 1972.

[25] Max–Planck–Institut für Eisenforschung und der Werkstoffausschuss des Vereins Deutscher Eisenhüttenleute, *Atlas zur Wärmebehandlung der Stähle, Teil I+II,* Verlag Stahleisen mbH, Düsseldorf, 1961.

[26] Scheil, E., *Anlaufzeit der Austenitumwandlung*, Arch. Eisenhüttenwes., 12 (1935), 565-567.

[27] Smallman, R. E., *Modern physical metallurgy*, Butterworths, London, 1985.

[28] Verdi, C., Visintin, A., *A mathematical model of the austenite-pearlite transformation in plain steel based on the Scheil's additivity rule*, Acta Metall., 35, No.11 (1987), 2711–2717.

[29] Visintin, A., *Mathematical Models of Solid-Solid Phase Transitions in Steel*, IMA J. Appl. Math., 39 (1987), 143-157.

[30] Visintin, A., *On supercooling and superheating effects in phase transitions*, Boll. U.M.I. Analalisi Funzionale e Applicazioni, Serie VI, Vol. V–C, No.1 (1986), 293–311.

Recent publications of the Weierstraß–Institut für Angewandte Analysis und Stochastik

Preprints 1994

115. Gerhard Häckl, Klaus R. Schneider: Controllability near Takens–Bogdanov points.

116. Tatjana A. Averina, Sergey S. Artemiev, Henri Schurz: Simulation of stochastic auto–oscillating systems through variable stepsize algorithms with small noise.

117. Joachim Förste: Zum Einfluß der Wärmeleitung und der Ladungsträgerdiffusion auf das Verhalten eines Halbleiterlasers.

118. Herbert Gajewski, Konrad Gröger: Reaction–diffusion processes of electrically charged species.

119. Johannes Elschner, Siegfried Prössdorf, Ian H. Sloan: The qualocation method for Symm's integral equation on a polygon.

120. Sergej Rjasanow, Wolfgang Wagner: A stochastic weighted particle method for the Boltzmann equation.

121. Ion G. Grama: On moderate deviations for martingales.

122. Klaus Fleischmann, Andreas Greven: Time–space analysis of the cluster–formation in interacting diffusions.

123. Grigori N. Milstein, Michael V. Tret'yakov: Weak approximation for stochastic differential equations with small noises.

124. Günter Albinus: Nonlinear Galerkin methods for evolution equations with Lipschitz continuous strongly monotone operators.

125. Andreas Rathsfeld: Error estimates and extrapolation for the numerical solution of Mellin convolution equations.

126. Mikhail S. Ermakov: On lower bounds of the moderate and Cramer type large deviation probabilities in statistical inference.

127. Pierluigi Colli, Jürgen Sprekels: Stefan problems and the Penrose–Fife phase field model.

128. Mikhail S. Ermakov: On asymptotic minimaxity of Kolmogorov and omega–square tests.

129. Gunther Schmidt, Boris N. Khoromskij: Boundary integral equations for the biharmonic Dirichlet problem on nonsmooth domains.

130. Hans Babovsky: An inverse model problem in kinetic theory.

131. Dietmar Hömberg: Irreversible phase transitions in steel.

132. Hans Günter Bothe: How 1–dimensional hyperbolic attractors determine their basins.

133. Ingo Bremer: Waveform iteration and one–sided Lipschitz conditions.

134. Herbert Gajewski, Klaus Zacharias: A mathematical model of emulsion polymerization.

135. J. Theodore Cox, Klaus Fleischmann, Andreas Greven: Comparison of interacting diffusions and an application to their ergodic theory.

136. Andreas Juhl: Secondary Euler characteristics of locally symmetric spaces. Results and Conjectures.

137. Nikolai N. Nefedov, Klaus R. Schneider, Andreas Schuppert: Jumping behavior in singularly perturbed systems modelling bimolecular reactions.

138. Roger Tribe, Wolfgang Wagner: Asymptotic properties of stochastic particle systems with Boltzmann type interaction.

Preprints 1995

139. Werner Horn, Jan Sokolowski, Jürgen Sprekels: Control problems with state constraints for the Penrose–Fife phase–field model.

140. Hans Babovsky: Simulation of kinetic boundary layers.

141. Ralf Kornhuber: A posteriori error estimates for elliptic variational inequalities.

142. Johannes Elschner, Youngmok Jeon, Ian H. Sloan, Ernst P. Stephan: The collocation method for mixed boundary value problems on domains with curved polygonal boundaries.

143. Johannes Elschner, Ernst P. Stephan: A discrete collocation method for Symm's integral equation on curves with corners.